



Stability of a modified Peaceman–Rachford method for the paraxial Helmholtz equation on adaptive grids [☆]



Qin Sheng ^{a,*}, Hai-wei Sun ^b

^a Department of Mathematics and Center for Astrophysics, Space Physics and Engineering Research, Baylor University, One Bear Place, Waco, TX 76798-7328, USA

^b Department of Mathematics, University of Macau, Macao

ARTICLE INFO

Article history:

Received 3 March 2016

Received in revised form 19 June 2016

Accepted 26 August 2016

Available online 31 August 2016

Keywords:

Paraxial wave approximations

High oscillations

Eikonal transformation

Splitting methods

Adaptive grids

Asymptotic stability

ABSTRACT

This study concerns the asymptotic stability of an eikonal, or ray, transformation based Peaceman–Rachford splitting method for solving the paraxial Helmholtz equation with high wave numbers. Arbitrary nonuniform grids are considered in transverse and beam propagation directions. The differential equation targeted has been used for modeling propagations of high intensity laser pulses over a long distance without diffractions. Self-focusing of high intensity beams may be balanced with the de-focusing effect of created ionized plasma channel in the situation, and applications of grid adaptations are frequently essential. It is shown rigorously that the fully discretized oscillation-free decomposition method on arbitrary adaptive grids is asymptotically stable with a stability index one. Simulation experiments are carried out to illustrate our concern and conclusions.

© 2016 Elsevier Inc. All rights reserved.

1. Introduction

While highly oscillatory wave problems pervade a wide range of applications in modern physics and technologies, the development of highly efficient and reliable computational strategies for them still remain as a serious concern. For instance, when highly oscillatory optical waves are considered, most existing numerical procedures require that the density of computational grids must be increased, or grid step sizes must be decreased, significantly, to meet the accuracy challenges [4,6,12,14,22,28].

Consider a typical electromagnetic field. The field can then be well described through charges and currents via Maxwell's field equations. In fact, together with the Lorentz force law, Maxwell's equations form the theoretical foundation of electrodynamics, modern optics and electric circuits. Although Maxwell's partial differential equations are not well suited for use in conventional initial-boundary value problem computations, if they are decoupled, we may acquire the following time-dependent Helmholtz equation which serves as an approximation to the underlying light [1,10,11,14]:

$$u_{tt} = c^2 (u_{xx} + u_{yy} + u_{zz}), \quad (x, y) \in \mathcal{D}_2, \quad z > z_0, \quad t > t_0, \quad (1.1)$$

[☆] This study was supported in part by a research leave award from Baylor University, and research grants No. MYRG102 (Y1-L3)-FST13-SHW from University of Macau and No. 105/2012/A3 from the FDCT of Macao.

* Principal and corresponding author.

E-mail addresses: Qin_Sheng@baylor.edu (Q. Sheng), hsun@umac.mo (H.-w. Sun).

where $u = u(x, y, z, t)$ is the intensity function of the field, z is the beam propagation direction, x, y are transverse directions perpendicular to the light, \mathcal{D}_2 is the two-dimensional convex domain. In the case when a monochromatic beam is concerned within a narrow cone [1,12], we may denote $u(x, y, z, t) = U(x, y, z, a)e^{2\pi i \nu t}$ for $(x, y, z) \in \mathcal{D}$, $t > t_0$, $\mathbf{i} = \sqrt{-1}$, ν is the frequency of the optical wave and U is the complex wave function with $\mathcal{D} = \mathcal{D}_2 \times \{z: z > z_0\}$. Substituting this into (1.1), we arrive immediately at

$$U_{xx} + U_{yy} + U_{zz} = -\kappa^2 U, \quad (x, y, z) \in \mathcal{D}, \quad (1.2)$$

where $\kappa = 2\pi\nu/c$ is the wave number, and c is the speed of light.

Further, let $E(x, y, z) = U(x, y, z)e^{ikz}$ be the complex envelope of U . Hence, from the time-independent Helmholtz equation (1.2) we observe that

$$2i\kappa E_z = E_{xx} + E_{yy} + E_{zz}, \quad (x, y, z) \in \mathcal{D}.$$

Let p denote the constant refractive parameter of the light system. If the change of the intensity of E in transverse directions is relatively slow, we may assume that $E_{zz} \approx \kappa^2 p E$ [10,11]. This leads to the paraxial Helmholtz equation,

$$2i\kappa E_z = E_{xx} + E_{yy} + \kappa^2 p E, \quad (x, y, z) \in \mathcal{D}. \quad (1.3)$$

Modern strategies for computing beam propagations can probably be traced back to the pioneering work of Stratton and Chu in diffraction integral approximations [14,25]. Since then, numerous numerical procedures, including the Fast Fourier Transform (FFT) based Beam Propagation Method (BPM), have been developed and studied for solving wave equations including (1.1)–(1.3) [10,11,28]. Among the most effective approaches implemented, there are spectral, pseudo-spectral, boundary element, finite-difference time-domain, multiresolution time-domain, local one-dimensional methods and optimized FFT-BPM formulations [15,17,20,21,29]. Remarkably accurate analytical algorithms have also been achieved via Richardson extrapolations and Lanczos recursive iterations, respectively [4,18]. When a high wave number is present, however, an existing conventional algorithm often becomes cumbersome due to the fact that its density of grids, or elements, employed in computational procedures must be increased significantly for meeting an accuracy requirement. This setback in the efficiency of computations inspires recent studies of fast algorithms for highly oscillatory differential equations and diffraction integrals [4–6,19–24,26].

Recent studies of the propagation of electromagnetic waves in the form of either paraboloidal waves or Gaussian beams reveal that, when paraxial optical waves, such as that described in (1.3), are targeted, the complex envelope of the electric field function can be approximated continuously through an eikonal, or ray, transformation originated from the geometric optics [1,11,13],

$$E(x, y, z) = \phi(x, y, z)e^{ik\psi(x, y, z)}, \quad (x, y, z) \in \bar{\mathcal{D}}, \quad (1.4)$$

where $\phi, \psi \in \mathbb{R}$. The above transformation effectively eliminates the need of high density computational grids and thus improves the overall efficiency. This has been particularly meaningful and practical in IR laser beam propagation simulations [9,12,17,28]. While different types of eikonal transformation based algorithms have emerged consequently [6,13–15,22,23], theoretical explorations of the strategy can be found in numerous recent publications [1,7,17,24].

It has been noticed, however, eikonal transformations may impair the numerical stability when the wave number κ involved is relatively low especially when mesh adaptations are used. This motivates our study on the asymptotic stability with respect to sensitive high wave numbers based on the unique matrix structure of the eikonal splitting algorithms. Our investigations ensure the high vibrance and applicability of the eikonal transformation based modified Peaceman–Rachford splitting for solving the highly oscillatory two-dimensional paraxial Helmholtz equation (1.3) on arbitrary grids.

Our discussions in this paper are organized as follows. In the next section, the discretization and splitting strategies of the eikonal transformation (1.4) based finite difference equations will be introduced. Details of the matrix structure of our scheme will be explored. Section 3 will be devoted to investigations of the asymptotic stability for the splitting strategy via rigorous matrix spectrum analysis. In Section 4, simulated numerical examples will be presented to illustrate the significance of the stability of computations on uniform and nonuniform adaptive grids. Concluding remarks will finally be given in Section 5.

2. Modified Peaceman–Rachford splitting on adaptive grids

Based on (1.4), the paraxial wave equation (1.3) can be decomposed to

$$\phi_z = \alpha (\psi_{xx} + \psi_{yy}) + f_1, \quad (1.5)$$

$$\psi_z = \beta (\phi_{xx} + \phi_{yy}) + f_2, \quad (1.6)$$

where ϕ, ψ are sufficiently smooth in $\bar{\mathcal{D}}$, $\phi \neq 0$, and

$$\alpha = \frac{\phi}{2}, \quad \beta = -\frac{1}{2\kappa^2\phi}, \quad f_1 = \phi_x\psi_x + \phi_y\psi_y, \quad f_2 = \frac{1}{2} [(\psi_x)^2 + (\psi_y)^2 - p]. \quad (1.7)$$

Let the functions in (2.3) be frozen. Then the solution of linearized differential equations (2.1), (2.2) are essentially non-oscillatory, as compared to (1.3), even when large values of κ are present. However, the solution pair ϕ, ψ may exhibit interesting near-singular patterns that need mesh adaptations via, say, an arc length monitoring or stretching mechanism [2,15].

Denote

$$w = \begin{bmatrix} \phi \\ \psi \end{bmatrix}, M = \begin{bmatrix} 0 & \alpha \\ \beta & 0 \end{bmatrix}, f = \begin{bmatrix} f_1 \\ f_2 \end{bmatrix}.$$

Then the coupled equations (2.1) and (2.2) can be combined to yield

$$w_z = M w_{xx} + M w_{yy} + f, \quad (x, y, z) \in \mathcal{D}. \tag{2.4}$$

Consider the adaptive mesh $\mathcal{D}_{h,\tau} = \left\{ (x_j, y_\ell, z_\sigma) : x_j = a + \sum_{k=0}^{j-1} h_{1,k}, y_\ell = c + \sum_{k=0}^{\ell-1} h_{2,k}, j, \ell = 0, 1, 2, \dots, n+1, x_{n+1} = b, y_{n+1} = d; z_\sigma = z_0 + \sum_{k=0}^{\sigma-1} \tau_k, \sigma = 0, 1, 2, \dots, L \right\}$, in which the nonuniform steps are determined via suitable monitoring functions such as the exponential evolving grids (EEG) formula [2,19], common moving mesh method [15], or z-stretching strategy [10,20] following standard smoothness constraints

$$\delta_1 \leq \frac{h_{1,k}}{h_{1,k+1}}, \frac{h_{2,k}}{h_{2,k+1}} \leq \delta_2, \quad k = 0, 1, \dots, n-1,$$

for given tolerances $\delta_1, \delta_2 > 0$. We may further denote that $0 < h_1 = \min_{0 \leq k \leq n} \{h_{1,k}\} \leq \max_{0 \leq k \leq n} \{h_{1,k}\} \ll 1, 0 < h_2 = \min_{0 \leq k \leq n} \{h_{2,k}\} \leq \max_{0 \leq k \leq n} \{h_{2,k}\} \ll 1$. Note that, due to its built-in flexibility, $\mathcal{D}_{h,\tau}$ can also be viewed as a general platform for different adaptive grids applications. Without loss of generality, we denote $\tau = \tau_k$ from hereon, and set

$$f_{i,j}^\sigma = (f_1(x_i, y_j, z_\sigma), f_2(x_i, y_j, z_\sigma))^T, \quad w_{i,j}^\sigma = (\phi(x_i, y_j, z_\sigma), \psi(x_i, y_j, z_\sigma))^T, \\ M_{i,j}^\sigma = \begin{bmatrix} 0 & \alpha_{i,j}^\sigma \\ \beta_{i,j}^\sigma & 0 \end{bmatrix}, \quad \alpha_{i,j}^\sigma = \frac{\phi(x_i, y_j, z_\sigma)}{2}, \quad \beta_{i,j}^\sigma = -\frac{1}{2\kappa^2 \phi(x_i, y_j, z_\sigma)}, \tag{2.5}$$

where $\max \phi \geq \phi(x_i, y_j, z_\sigma) \geq \min \phi > 0, (x_i, y_j, z_\sigma) \in \mathcal{D}_{h,\tau}$, in which both $\min \phi$ and $\max \phi$ are independent of n [1,21]. We adopt following nonuniform finite difference approximations [2,4],

$$h_1^2 (w_{xx})_{i,j}^\sigma = p_{1,i} w_{i-1,j}^\sigma - r_{1,i} w_{i,j}^\sigma + q_{1,i} w_{i+1,j}^\sigma - \frac{h_{1,i} - h_{1,i-1}}{3} h_1^2 (w_{xxx})_{i,j} \\ - \frac{h_{1,i}^2 - h_{1,i} h_{1,i-1} + h_{1,i-1}^2}{12} h_1^2 (w_{xxxx})_{i,j}^\sigma + \mathcal{O}(h_1^5), \\ h_2^2 (w_{yy})_{i,j}^\sigma = p_{2,j} w_{i,j-1}^\sigma - r_{2,j} w_{i,j}^\sigma + q_{2,j} w_{i,j+1}^\sigma - \frac{h_{2,j} - h_{2,j-1}}{3} h_2^2 (w_{yyy})_{i,j} \\ - \frac{h_{2,j}^2 - h_{2,j} h_{2,j-1} + h_{2,j-1}^2}{12} h_2^2 (w_{yyyy})_{i,j}^\sigma + \mathcal{O}(h_2^5),$$

in which

$$p_{s,k} = \frac{2h_s^2}{h_{s,k-1}(h_{s,k-1} + h_{s,k})}, \quad r_{s,k} = \frac{2h_s^2}{h_{s,k-1}h_{s,k}}, \quad q_{s,k} = \frac{2h_s^2}{h_{s,k}(h_{s,k-1} + h_{s,k})}, \\ s = 1, 2; \quad k = 1, 2, \dots, n.$$

Suppose that suitable initial and Dirichlet boundary conditions are imposed. We derive from (2.4) the following semi-discretized system,

$$\tau w'(z_\sigma) = A^\sigma w(z_\sigma) + B^\sigma w(z_\sigma) + \tau f(z_\sigma), \quad z_\sigma > z_0; \quad w(z_0) = g_0, \tag{2.6}$$

where $A^\sigma = \mu_1 M^\sigma T_1, B^\sigma = \mu_2 M^\sigma T_2, \mu_s = \tau/h_s^2 \leq c, s = 1, 2, \tau > 0$, and

$$M^\sigma = \text{diag}(M_1^\sigma, M_2^\sigma, \dots, M_n^\sigma) \in \mathbb{R}^{2n^2 \times 2n^2} \tag{2.7}$$

with

$$M_j^\sigma = \text{diag}(M_{1,j}^\sigma, M_{2,j}^\sigma, \dots, M_{n,j}^\sigma), \quad j = 1, 2, \dots, n,$$

and

$$T_1 = I_n \otimes R_1 \otimes I_2, \quad T_2 = R_2 \otimes I_2 \otimes I_n,$$

where $I_k \in \mathbb{R}^{k \times k}$ is the identity matrix, with weakly diagonally dominant and irreducible matrices

$$R_1 = \begin{bmatrix} -r_{1,1} & q_{1,1} & & & & \\ p_{1,2} & -r_{1,2} & q_{1,2} & & & \\ & \ddots & \ddots & \ddots & & \\ & & & p_{1,n} & -r_{1,n} & \end{bmatrix}, \quad R_2 = \begin{bmatrix} -r_{2,1} & q_{2,1} & & & & \\ p_{2,2} & -r_{2,2} & q_{2,2} & & & \\ & \ddots & \ddots & \ddots & & \\ & & & p_{2,n} & -r_{2,n} & \end{bmatrix}.$$

The vector f contains contributions from the source term in (2.4) and boundary functions, that is, $f(z_\sigma) = ((f_{1,1}^\sigma + g_{1,1}^\sigma)^\top, (f_{2,1}^\sigma + g_{2,1}^\sigma)^\top, \dots, (f_{n,1}^\sigma + g_{n,1}^\sigma)^\top, (f_{1,2}^\sigma + g_{1,2}^\sigma)^\top, (f_{2,2}^\sigma + g_{2,2}^\sigma)^\top, \dots, (f_{n,2}^\sigma + g_{n,2}^\sigma)^\top, \dots, (f_{1,n}^\sigma + g_{1,n}^\sigma)^\top, (f_{2,n}^\sigma + g_{2,n}^\sigma)^\top, \dots, (f_{n,n}^\sigma + g_{n,n}^\sigma)^\top)^\top$, where

$$\begin{aligned} g_{1,k}^\sigma &= p_{1,k}^\sigma w_{0,k}^\sigma, \quad g_{n,k}^\sigma = q_{1,k}^\sigma w_{n+1,k}^\sigma; \quad g_{k,1}^\sigma = p_{2,k}^\sigma w_{k,0}^\sigma, \quad g_{k,n}^\sigma = q_{2,k}^\sigma w_{k,n+1}^\sigma, \quad k = 2, 3, \dots, n-1, \\ g_{1,1}^\sigma &= p_{1,1}^\sigma w_{0,1}^\sigma + p_{2,1}^\sigma w_{1,0}^\sigma, \quad g_{1,n}^\sigma = p_{1,1}^\sigma w_{0,1}^\sigma + p_{2,n}^\sigma w_{n+1,0}^\sigma, \\ g_{n,1}^\sigma &= p_{1,n}^\sigma w_{n+1,1}^\sigma + p_{2,1}^\sigma w_{1,0}^\sigma, \quad g_{n,n}^\sigma = p_{1,n}^\sigma w_{n+1,1}^\sigma + p_{2,n}^\sigma w_{1,n+1}^\sigma, \\ g_{i,j}^\sigma &\equiv 0 \text{ if neither } i \text{ nor } j \text{ is } 1 \text{ or } n, \end{aligned}$$

where $w_{i,j}^\sigma$, $i \in \{0, n+1\}$ or $j \in \{0, n+1\}$, are boundary values based on the variable transverse grids at the level of σ in the beam propagation direction.

Remark 2.1. Based on the nonuniform finite difference approximations utilized, the local truncation error of the scheme (2.6) is in general of the size $\mathcal{O}(h)$ as $h \rightarrow 0$, where $h = \max\{h_1, h_2\}$.

Lemma 2.1. We have $\|R_1\|_2, \|R_2\|_2 \leq 4$.

Proof. The proof of the lemma is straightforward based on a norm triangular inequality and definitions of h_s , $s = 1, 2$. \square

With an initial vector w^0 , the formal solution of (2.6) can be expressed recursively as

$$w^{\sigma+1} = e^{\mu_1 A^\sigma + \mu_2 B^\sigma} w^\sigma + \tau \int_0^1 e^{(1-\xi)(\mu_1 A^\sigma + \mu_2 B^\sigma)} f((\sigma + \xi)\tau) d\xi, \quad \sigma = 0, 1, 2, \dots$$

For a sufficiently small z -step $\tau > 0$, we replace the integral by a left-end quadrature to yield

$$w^{\sigma+1} \approx e^{\mu_1 A^\sigma + \mu_2 B^\sigma} (w^\sigma + \tau f^\sigma), \quad \sigma = 0, 1, 2, \dots$$

Hence, an application of the Peaceman-Rachford formula [19] for the above leads to the following conventional splitting scheme,

$$\begin{aligned} w^{\sigma+1} &= (I_{2n^2} - \mu_2 B^\sigma) (I_{2n^2} + \mu_1 A^\sigma) (I_{2n^2} - \mu_1 A^\sigma) (I_{2n^2} + \mu_2 B^\sigma) (w^\sigma + \tau f^\sigma), \\ \sigma &= 0, 1, 2, \dots, \end{aligned}$$

which can be improved to our modified method via a modification similar to Steffensen's acceleration,

$$\begin{aligned} w^{\sigma+1} &= (I_{2n^2} - \mu_2 B^{\sigma+1/2}) (I_{2n^2} + \mu_1 A^{\sigma+1/2}) (I_{2n^2} - \mu_1 A^\sigma) (I_{2n^2} + \mu_2 B^\sigma) \\ &\times (w^\sigma + \tau f^\sigma), \quad \sigma = 0, 1, 2, \dots \end{aligned}$$

The above splitting algorithm can also be decoupled to a two-stage systems,

$$(I_{2n^2} - \mu_1 A^\sigma) w^{\sigma+1/2} = (I_{2n^2} + \mu_2 B^\sigma) w^\sigma + \frac{\tau}{2} g^\sigma, \tag{2.8}$$

$$\begin{aligned} (I_{2n^2} - \mu_2 B^{\sigma+1/2}) w^{\sigma+1} &= (I_{2n^2} + \mu_1 A^{\sigma+1/2}) w^{\sigma+1/2} + \frac{\tau}{2} g^{\sigma+1/2}, \tag{2.9} \\ (x_i, y_j, z_\sigma) &\in \mathcal{D}_{h,\tau} \end{aligned}$$

where

$$\begin{aligned} g^k &= (g_{1,1}^k, g_{2,1}^k, \dots, g_{n,1}^k, g_{1,2}^k, g_{2,2}^k, \dots, g_{n,2}^k, \dots, g_{n,n}^k)^\top \in \mathbb{R}^{2n^2}, \\ w^k &= (w_{1,1}^k, w_{2,1}^k, \dots, w_{n,1}^k, w_{1,2}^k, w_{2,2}^k, \dots, w_{n,2}^k, \dots, w_{n,n}^k)^\top \in \mathbb{R}^{2n^2}. \end{aligned}$$

We note that the modified Peaceman–Rachford splitting is of order-one in approximations due to the nonuniform mesh finite differences utilized. The new scheme can be further compressed to

$$w^{\sigma+1} = Q^{\sigma+1/2} P^\sigma w^\sigma + \frac{\tau}{2} g_0^\sigma, \tag{2.10}$$

where

$$P^\sigma = (I_{2n^2} - \mu_1 A^\sigma)^{-1} (I_{2n^2} + \mu_2 B^\sigma), \tag{2.11}$$

$$Q^{\sigma+1/2} = (I_{2n^2} - \mu_2 B^{\sigma+1/2})^{-1} (I_{2n^2} + \mu_1 A^{\sigma+1/2}), \tag{2.12}$$

$$g_0^\sigma = Q^{\sigma+1/2} (I_{2n^2} - \mu_1 A^\sigma)^{-1} g^\sigma + (I_{2n^2} - \mu_2 B^{\sigma+1/2})^{-1} g^{\sigma+1/2}.$$

We further notice that $Q^{\sigma+1/2} P^\sigma$ also plays the role of an amplification matrix for our scheme. Apparently, the modified Peaceman–Rachford scheme (2.8), (2.9), or (2.10), represents a group of adaptive splitting methods due to a high flexibility of computational grids.

Remark 2.2. Since a left-end quadrature is employed for approximating the formal solution, the local truncation error of the fully discretized system (2.8), (2.9), or (2.10), is of the size $\mathcal{O}(\tau + h)$ as $\tau, h \rightarrow 0$, where $h = \max\{h_1, h_2\}$. We also note that the Peaceman–Rachford splitting utilized cannot lead to conventional second order approximations in the scenario due to the use of adaptive transverse step sizes [2].

Although discussions of similar numerical procedures for solving (2.4) can be found in a number of recent publications (for instance, see [3,21,28] and references therein), more general studies of eikonal transformation based numerical methods for solving highly oscillatory problems, especially when adaptive grids are incorporated, are still in infancy [2,10,16,21,26].

3. Asymptotic stability

It has been observed in recent computational experiments that instabilities may occur when (2.10) is used for long z-distance executions with smaller wave numbers [13,21,22]. Although this may not affect applications of eikonal transformation based algorithms in high frequency optical wave computations, rigorous analysis of stability for the numerical methods are still appropriate and necessary. In Fig. 3.1, a typical long z-distance simulation example is given. An eikonal splitting scheme is utilized for calculating a Gaussian beam type wave solution E of (1.3) up to z-level 1000. The breakdown of the stability of the modulus function becomes visible at the z-level 925, and the solution loses its true identity by the z-level 1000.

Definition 1. [6,21] Consider a finite difference method with an amplification matrix Φ for solving (2.1), (2.2) associated with an oscillatory wave problem. κ is the large wavenumber involved. We say that the numerical method is asymptotically stable if there exists positive constants c, d independent of κ such that

$$\rho(\Phi) \leq 1 + c\kappa^{-d}, \quad \kappa \rightarrow \infty,$$

where $\rho(\cdot)$ is the spectral radius and $d_0 = \sup\{d\}$ is the asymptotical stability index of the numerical method.

Remark 3.1. The above definition is designed for linearized numerical methods in a localized sense. Discussions of more vibrant nonlinear stabilities can be found in a number of recent publications (for example, see [6,26] and references therein). Applications of Lyapunov functionals are often necessary. Since we are primarily interested in asymptotic behaviors of the system (2.1)–(2.3) after its nonlinear coefficients and terms being frozen, the use of Definition 1 becomes meaningful and justified.

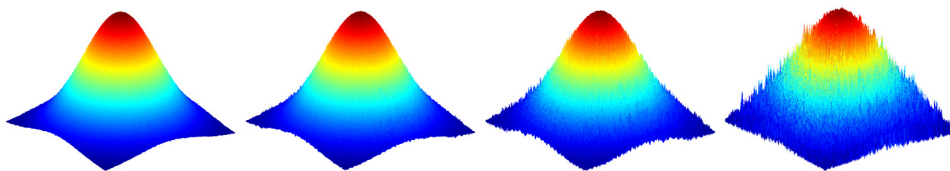


Fig. 3.1. A typical evolution profile of the instability of an eikonal transformation based scheme when a relatively small $\kappa = 10$ is utilized in long distance computations. Modulus of the wave solution E is plotted at the z-level 900, 925, 975 and 1000 (from left to right). A Gaussian beam type initial condition and homogeneous Neumann boundary conditions are used. The stability can be improved significantly if bigger κ values are considered.

Let us now analyze our amplification matrix $Q^{\sigma+1/2}P^\sigma$ introduced by (2.10). To this end, we denote

$$P = [e_1, e_3, \dots, e_{2n^2-1}, e_2, e_4, \dots, e_{2n^2}] \in \mathbb{R}^{2n^2 \times 2n^2},$$

where e_j is the j th column of the $2n^2 \times 2n^2$ identity matrix, be a permutation matrix. From (2.7) we observe that

$$P^T M^\sigma P = \begin{bmatrix} 0 & \Lambda_\alpha^\sigma \\ \Lambda_\beta^\sigma & 0 \end{bmatrix},$$

where

$$\Lambda_\alpha^\sigma = \text{diag}(\alpha_{1,1}^\sigma, \alpha_{2,1}^\sigma, \dots, \alpha_{n,1}^\sigma, \alpha_{1,2}^\sigma, \dots, \alpha_{n,n}^\sigma),$$

$$\Lambda_\beta^\sigma = \text{diag}(\beta_{1,1}^\sigma, \beta_{2,1}^\sigma, \dots, \beta_{n,1}^\sigma, \beta_{1,2}^\sigma, \dots, \beta_{n,n}^\sigma),$$

and $\alpha_{i,j}^\sigma$ and $\beta_{i,j}^\sigma$ are due to (2.5). Further, for the simplicity of notations, let c_k , $k = 0, 1, 2, \dots$, denote positive constants independent of κ . Thus, based on definitions of the above matrices, we have

$$\|\Lambda_\alpha^\sigma\|_2 = \frac{\max \phi}{2} \leq c_1, \quad \|\Lambda_\beta^\sigma\|_2 = \frac{1}{2\kappa^2 \min \phi} \leq c_2 \kappa^{-2}, \quad \kappa \rightarrow \infty. \tag{3.1}$$

Further,

$$P^T T_1 P = I_2 \otimes I_n \otimes R_1 \quad \text{and} \quad P^T T_2 P = I_2 \otimes R_2 \otimes I_n.$$

Set

$$K_\sigma = P^T A^\sigma P = P^T M^\sigma T_1 P = \begin{bmatrix} 0 & \Lambda_\alpha^\sigma(I_n \otimes R_1) \\ \Lambda_\beta^\sigma(I_n \otimes R_1) & 0 \end{bmatrix}, \tag{3.2}$$

$$L_\sigma = P^T B^\sigma P = P^T M^\sigma T_2 P = \begin{bmatrix} 0 & \Lambda_\alpha^\sigma(R_2 \otimes I_n) \\ \Lambda_\beta^\sigma(R_2 \otimes I_n) & 0 \end{bmatrix}. \tag{3.3}$$

Recall that $\|R_1\|_2, \|R_2\|_2 \leq 4$, it follows immediately that

$$\|I_n \otimes R_1\|_2 = \|R_1\|_2 \leq 4, \quad \|R_2 \otimes I_n\|_2 = \|R_2\|_2 \leq 4, \quad \kappa \rightarrow \infty. \tag{3.4}$$

On the other hand, we may show

Lemma 3.1. *The spectra of M^σ and N^σ are bounded by $c_3 \kappa^{-1}$.*

Proof. We first show that $\|K_\sigma^2\|_2 \leq c_4 \kappa^{-2}$. To see this, from (3.2) we acquire that

$$K_\sigma^2 = \begin{bmatrix} \Lambda_\alpha^\sigma(R_1 \otimes I_n) \Lambda_\beta^\sigma(R_1 \otimes I_n) & 0 \\ 0 & \Lambda_\beta^\sigma(R_1 \otimes I_n) \Lambda_\alpha^\sigma(R_1 \otimes I_n) \end{bmatrix}.$$

Hence, due to (3.1) and (3.4),

$$\|K_\sigma^2\|_2 \leq \|\Lambda_\alpha^\sigma\|_2 \|R_1 \otimes I_n\|_2 \|\Lambda_\beta^\sigma\|_2 \|R_1 \otimes I_n\|_2 \leq c_4 \kappa^{-2}, \quad \kappa \rightarrow \infty, \tag{3.5}$$

which implies the bounds $\rho(M^\sigma) = \rho(K_\sigma) \leq c_3 \kappa^{-1}$. Analogously, by (3.3), we have $\|L_\sigma^2\|_2 \leq c_5 \kappa^{-2}$ and therefore $\rho(N^\sigma) = \rho(L_\sigma) \leq c_3 \kappa^{-1}$. \square

Similarly,

$$K_\sigma K_\sigma^T = (I_{2n} \otimes R_1) \begin{bmatrix} (\Lambda_\alpha^\sigma)^2 & 0 \\ 0 & (\Lambda_\beta^\sigma)^2 \end{bmatrix} (I_{2n} \otimes R_1).$$

Thus, by applying estimates (3.1) and (3.4), we obtain that

$$\|K_\sigma\|_2 = \sqrt{\rho(K_\sigma K_\sigma^T)} \leq \sqrt{4^2 \rho((\Lambda_\alpha^\sigma)^2)} \leq c_6, \quad \kappa \rightarrow \infty.$$

The estimate $\|L_\sigma\|_2 \leq c_6$ comes analogously.

On the other hand, it is observed in (2.11) that P^σ can be decomposed to yield

$$P^\sigma = (I_{2n^2} - \mu_1 A^\sigma)^{-1} (I_{2n^2} + \mu_2 B^\sigma) = I_{2n^2} + (I_{2n^2} - \mu_1 A^\sigma)^{-1} (\mu_2 B^\sigma + \mu_1 A^\sigma).$$

Since μ_1, μ_2 are finite and $\kappa \gg 10$ in common optical wave applications, we may assume that

$$\frac{\mu_1}{\kappa} \ll 1, \frac{\mu_2}{\kappa} \ll 1.$$

Hence,

$$\begin{aligned} P^T (I_{2n^2} - \mu_1 A^\sigma)^{-1} (\mu_2 B^\sigma + \mu_1 A^\sigma) P &= (I_{2n^2} - \mu_1 K_\sigma)^{-1} (\mu_2 L_\sigma + \mu_1 K_\sigma) \\ &= \mu_1 \left(I_{2n^2} - \mu_1^2 K_\sigma^2 \right)^{-1} K_\sigma (\mu_2 L_\sigma + \mu_1 K_\sigma) \\ &\quad + \left(I_{2n^2} - \mu_1^2 K_\sigma^2 \right)^{-1} (\mu_2 L_\sigma + \mu_1 K_\sigma) = C^{-1} (M_1 + M_2), \end{aligned} \tag{3.6}$$

where

$$\begin{aligned} C &= \begin{bmatrix} C_1 & 0 \\ 0 & C_2 \end{bmatrix}, \\ C_1 &= I_{n^2} - \mu_1^2 \Lambda_\alpha^\sigma (I_n \otimes R_1) \Lambda_\beta^\sigma (I_n \otimes R_1), \\ C_2 &= I_{n^2} - \mu_1^2 \Lambda_\beta^\sigma (I_n \otimes R_1) \Lambda_\alpha^\sigma (I_n \otimes R_1), \\ M_1 &= \mu_1 K_\sigma (\mu_2 L_\sigma + \mu_1 K_\sigma), \\ M_2 &= \mu_1 K_\sigma + \mu_2 L_\sigma = \begin{bmatrix} 0 & \Lambda_\alpha^\sigma \\ \Lambda_\beta^\sigma & 0 \end{bmatrix} R, \end{aligned}$$

in which $R = \mu_1 I_n \otimes R_1 + \mu_2 R_1 \otimes I_n$ and thus, consequently, $\|R\|_2 \leq c_0(\mu_1 + \mu_2)$.

Lemma 3.2. Let $\kappa \rightarrow \infty$. We have

- (i) $\|C^{-1}\|_2 \leq c_0$, and consequently $\|C_1^{-1}\|_2 \leq c_1$, $\|C_2^{-1}\|_2 \leq c_2$;
- (ii) $\|C^{-1}M_1\|_2 \leq c_3(\mu_1^2 + \mu_2^2)\kappa^{-2}$;
- (iii) $\|M_2\|_2 \leq c_4(\mu_1 + \mu_2)$;
- (iv) $\|(C^{-1}M_2)^2\|_2 \leq c_5(\mu_1^2 + \mu_2^2)\kappa^{-2}$.

Proof. Recall (3.5),

$$\|C\|_2 \geq 1 - \mu_1^2 \|K_\sigma^2\|_2 \geq 1 - c_5 \mu_1^2 \kappa^{-2}, \quad \kappa \rightarrow \infty.$$

Since $\mu_1/\kappa \ll 1$, we conclude readily that $\|C^{-1}\|_2 \leq c_0$. Subsequently, $\|C_1^{-1}\|_2 \leq c_1$, $\|C_2^{-1}\|_2 \leq c_2$ for some positive constants. For the product

$$K_\sigma L_\sigma = \begin{bmatrix} \Lambda_\alpha^\sigma (I_n \otimes R_1) \Lambda_\beta^\sigma (R_2 \otimes I_n) & 0 \\ 0 & \Lambda_\beta^\sigma (I_n \otimes R_1) \Lambda_\alpha^\sigma (R_2 \otimes I_n) \end{bmatrix},$$

apparently we have $\|K_\sigma L_\sigma\|_2 \leq c_3 \kappa^{-2}$ according to (3.1). It follows therefore

$$\|C^{-1}M_1\|_2 = \|C^{-1}(\mu_1 \mu_2 K_\sigma L_\sigma + \mu_1^2 K_\sigma^2)\|_2 \leq c_4(\mu_1^2 + \mu_2^2)\kappa^{-2}$$

due to the fact that

$$\|K_\sigma^2\|_2 \leq \kappa^{-2}.$$

We further observe that

$$\|M_2\|_2 = \sqrt{\rho(M_2 M_2^T)} = \sqrt{\rho(R(\Lambda_\alpha^\sigma)^2 R)} \leq c_5(\mu_1 + \mu_2), \quad \kappa \rightarrow \infty.$$

On the other hand, a straightforward calculation shows that

$$C^{-1}M_2 = \begin{bmatrix} 0 & C_2^{-1} \Lambda_\alpha R \\ C_1^{-1} \Lambda_\beta R & 0 \end{bmatrix}.$$

Thus,

$$(C^{-1}M_2)^2 = \begin{bmatrix} C_2^{-1} \Lambda_\alpha R C_1^{-1} \Lambda_\beta R & 0 \\ 0 & C_1^{-1} \Lambda_\beta R C_2^{-1} \Lambda_\alpha R \end{bmatrix}.$$

Recall that $\|C_1^{-1}\|_2 \leq c_1$, $\|C_2^{-1}\|_2 \leq c_2$, $\|\Lambda_\alpha\|_2 \leq c_3$, $\|R\|_2 \leq c_4(\mu_1 + \mu_2)$ and $\|\Lambda_\beta\|_2 \leq c_5 \kappa^{-2}$ for some positive constants c_k , $k = 1, 2, \dots, 5$. These lead to,

$$\|(C^{-1}M_2)^2\|_2 \leq \|C_2^{-1}\|_2 \|\Lambda_\alpha\|_2 \|R\|_2 \|C_1^{-1}\|_2 \|\Lambda_\beta\|_2 \|R\|_2 \leq c_6 (\mu_1^2 + \mu_2^2) \kappa^{-2}, \quad \kappa \rightarrow \infty.$$

This completes our proof. \square

Theorem 3.1. *The eikonal transformation based modified Peaceman–Rachford method (2.8), (2.9), or (2.10), on arbitrary adaptive grids is oscillation-free and asymptotically stable with a stability index one.*

Proof. The first claim is secured by our ray transformation formula. Now, recall (3.6) and that $Q^{\sigma+1/2}P^{\sigma}$ is our amplification matrix. By using Lemma 3.2 we observe that

$$\begin{aligned} & \left\| \left(P^{\top} (I_{2n^2} - \mu_1 A^{\sigma})^{-1} (\mu_2 B^{\sigma} + \mu_1 A^{\sigma}) P \right)^2 \right\|_2 \\ &= \|(C^{-1}M_1)^2 + (C^{-1}M_2)^2 + C^{-1}M_1C^{-1}M_2 + C^{-1}M_2C^{-1}M_1\|_2 \\ &\leq \|(C^{-1}M_1)^2\|_2 + \|(C^{-1}M_2)^2\|_2 + \|C^{-1}\|_2\|M_1\|_2\|C^{-1}\|_2\|M_2\|_2 \\ &\quad + \|C^{-1}\|_2\|M_2\|_2\|C^{-1}\|_2\|M_1\|_2 \leq c_0(\mu_1^3 + \mu_2^3)\kappa^{-2}, \quad \kappa \rightarrow \infty. \end{aligned}$$

The above inequalities ensure the following bound,

$$\rho(P^{\sigma}) = 1 + \rho \left((I_{2n^2} - \mu_1 A^{\sigma})^{-1} (\mu_2 B^{\sigma} + \mu_1 A^{\sigma}) \right) \leq 1 + c_7(\mu_1 + \mu_2)^{3/2}\kappa^{-1}, \quad \kappa \rightarrow \infty.$$

Now, recall (2.12). By the same token, we can show similarly that

$$\rho(Q^{\sigma}) \leq 1 + c_8(\mu_1 + \mu_2)^{3/2}\kappa^{-1}, \quad \kappa \rightarrow \infty.$$

The investigation indicates that if both μ_1 and μ_2 are bounded, then the eikonal transformation based splitting methods on arbitrary grids, which are determined via proper adaptations, must be asymptotically stable with an asymptotical stability index one. This completes our proof. \square

Remark 3.2. Though strong numerical evidences have indicated that, if the classical linear stability of an eikonal transformation based splitting scheme exists on the z-direction under suitable norms, it should be conditional. The constraints required must depend on the wave number κ . Rigorous mathematical proofs of such claims are still expected.

4. Computational experiments

There has been a significant amount of recent publications in highly oscillatory wave computations. Straightforward applications of typical splitting strategies, such as the LOD and ADI methods, can be found in [5,6,22–24,29]. Spectrum and

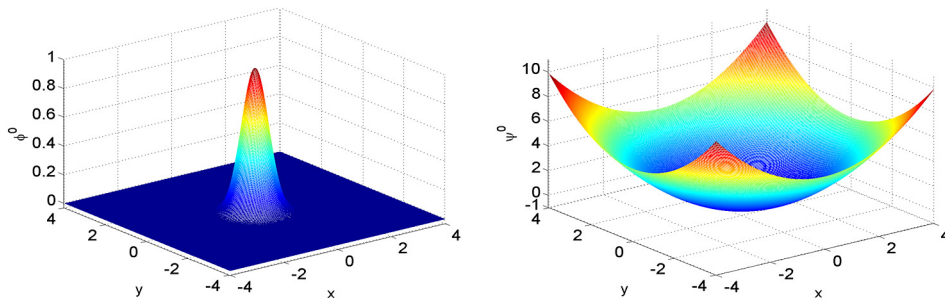


Fig. 4.1. A three-dimensional view of a typical pair of Gaussian beam initial functions ϕ^0 (left) and ψ^0 (right). The frequency $\kappa = 1$ and homogeneous Neumann boundary conditions are utilized. Both ϕ^0 and ψ^0 exhibit nice smoothness without oscillations.

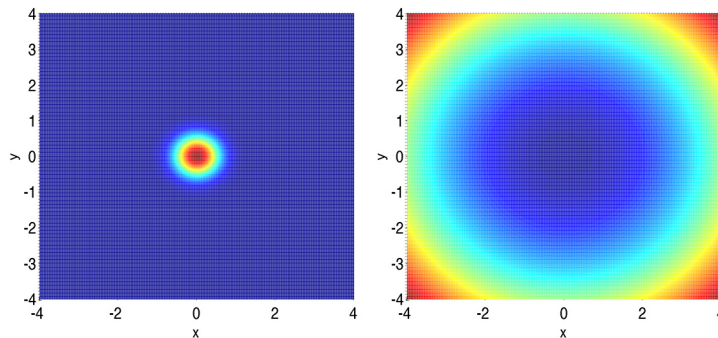


Fig. 4.2. Contour maps of initial functions ϕ^0 (left) and ψ^0 (right). It can be observed that, though both functions exhibit nice smoothness, they change rapidly in central transverse areas. Apparently, variable, or adaptive, transverse grids are more preferably for better numerical approximations.

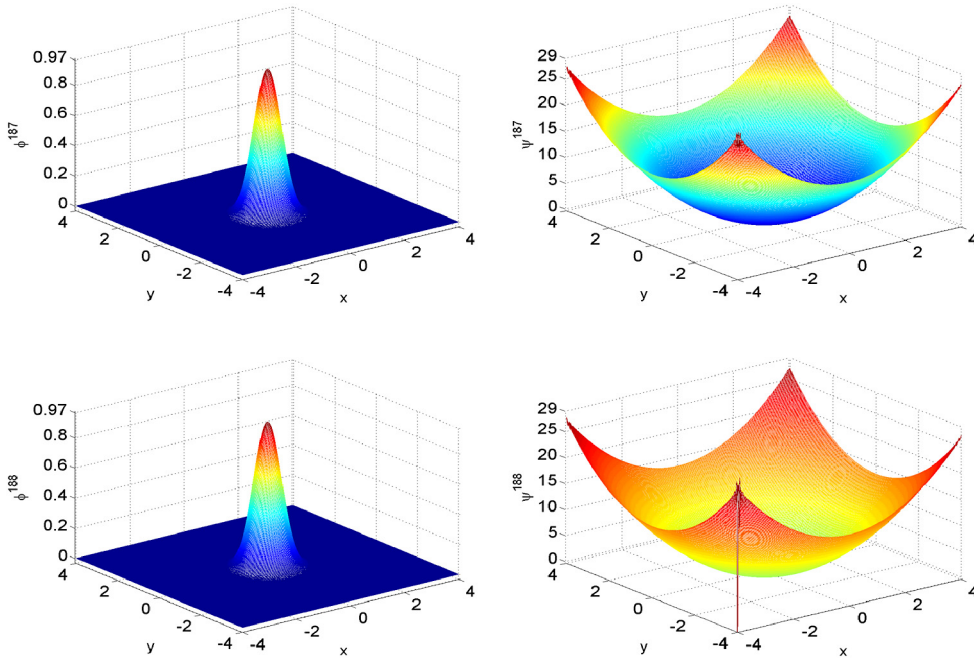


Fig. 4.3. Three-dimensional views of numerical solutions ϕ^{187} , ψ^{187} (top) and ϕ^{188} , ψ^{188} (bottom). The frequency with $\kappa = 1$ and a CFL number approximately 0.025 on fine uniform grids are utilized. Homogeneous Neumann boundary conditions are considered. Instability disturbances start to be visible, especially around some corners of the transverse domain especially for ψ when $\sigma > 180$. The errors built-up may due to the use of eikonal transformation based method in small wave number circumstances.

finite element strategies reinforced by parallel computations are also studied [3,6,27]. In most existing procedures, however, mesh step sizes utilized are inversely proportional to the wave number κ used [5,6,13,14]. For the reason, mathematically profound formulations are often difficult to realize for practical or industrial applications. This has motivated the eikonal transformation based algorithms which effectively eliminate high oscillation components. As a consequence, grid step sizes become independent of κ and thus can be chosen to be sufficiently large for faster calculations. Although this breaks the traditional efficiency barrier, the eikonal method may introduce additional errors and instabilities when κ values are relatively small. Our following experiments, using only a fraction amount of the computational time in [8,9], are particularly designed to illustrate the importance of the stability in computations.

Example 4.1. Consider a typical Gaussian beam type initial function

$$u(x, y, z_0) = \frac{1}{1 + iz_0} \exp \left\{ -\frac{x^2 + y^2}{2r_0^2(1 + iz_0)} \right\}, \quad -\ell_0 \leq x, y \leq \ell_0, \tag{4.1}$$

where $z_0 = 2\pi r_0^2/\lambda$ [9]. The input function is standard in the vector diffraction theory as well as laboratorial experiments [1,13,21]. Recalling (1.4), we may equivalently express (4.1) in the eikonal form, that is,

$$u(x, y, z_0) = \phi^0(x, y, z_0) \exp \left\{ ik \psi^0(x, y, z_0) \right\}, \quad -\ell_0 \leq x, y \leq \ell_0.$$

A straightforward calculation indicates that

$$\phi^0(x, y, z_0) = \frac{1}{\sqrt{1 + z_0^2}} \exp \left\{ -\frac{x^2 + y^2}{2r_0^2(1 + z_0^2)} \right\}, \tag{4.2}$$

$$\psi^0(x, y, z_0) = \frac{(x^2 + y^2)z_0}{2(1 + z_0^2)} - r_0^2 \cos^{-1} \left(\frac{1}{\sqrt{1 + z_0^2}} \right). \tag{4.3}$$

Now, consider a low frequency $\kappa = 1$ and set $\ell_0 = 4$. Adopt natural homogeneous Neumann boundary conditions on the transverse boundary. We show functions $\phi^0(x, y, z_0)$ and $\psi^0(x, y, z_0)$ in Fig. 4.1. Their contour maps on the transverse plane are given in Fig. 4.2. Although both ϕ^0 and ψ^0 exhibit nice and smooth patterns, the functions values, especially that

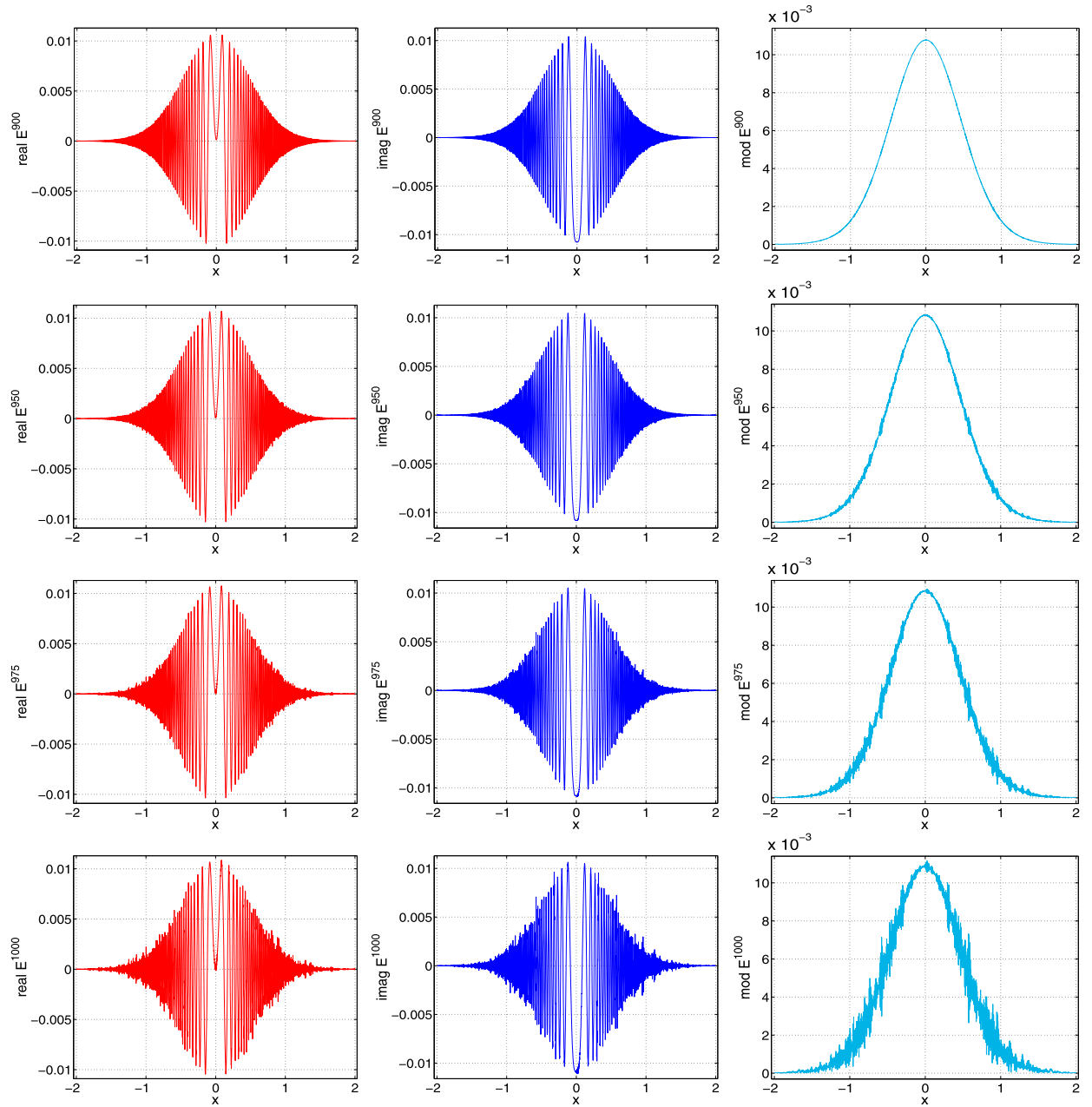


Fig. 4.4. Two-dimensional projections of the real, imaginary parts and modules of the numerical solution E^σ . $\sigma = 900, 950, 975, 1000$ (from top to bottom) are plotted. $\kappa = 10$ is used. Fixed nonuniform transverse grids are introduced for all z -level computations. Apparently, the stability of the modified eikonal transformation based Peaceman–Rachford scheme (2.10) is improved remarkably when a larger κ value is utilized. The instability disturbances still appear, though.

for ϕ^0 , change rapidly in central transverse areas. Variable, or adaptive, transverse grids clearly have an edge over traditional uniform grids in numerical approximations.

In Fig. 4.3, we show the pair of numerical solutions ϕ^σ, ψ^σ of (2.10) as the z -step σ reaches steps 187, 188, respectively. It is noticed that disturbances due to numerical instabilities become easily visible and errors built-up lead to a major break-down of the entire computed solution at the z -step $\sigma = 189$. The problem occurs initially around some corners of the transverse region.

The unfavorable instability shown in this example as well as in our other simulation experiments indicates that the eikonal Peaceman–Rachford splitting method may not be stable in cases when relatively small wave numbers are considered in flow computations. Therefore the use of the numerical method needs to be extremely careful. The stability concern promotes the study of asymptotical stability with $\kappa \gg 1$ for optical applications where large wave numbers are common.

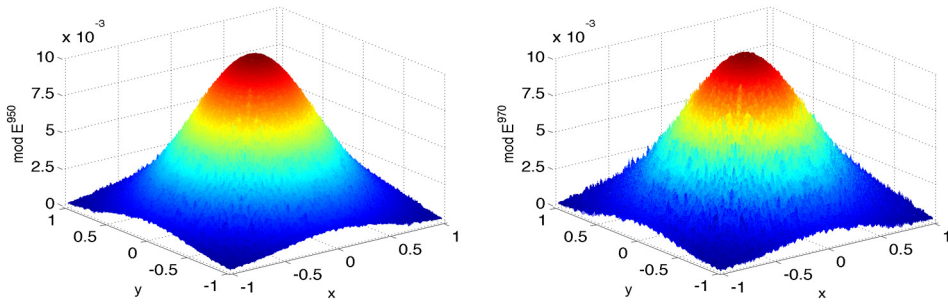


Fig. 4.5. Three-dimensional views of the modules of E^{950} (left) and E^{970} (right). The frequency at $\kappa = 10$ is utilized, and a locally enlarged viewing domain $-1 \leq x, y \leq 1$ is adopted in the transverse plain for showing more details. Fine nonuniform grids are considered. Erroneous disturbances are clearly visible throughout the solution surfaces after long z -distance computations.

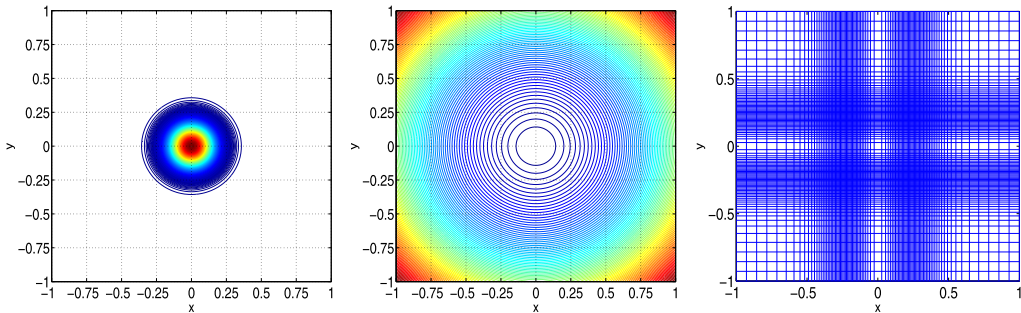


Fig. 4.6. Contour maps of the symmetric solutions ϕ^{100} (left) and ψ^{100} (center). The corresponding symmetric nonuniform grids (right) are generated via an arc length adaptive formula via monitoring function [2]. The mesh follows nicely the pattern of both solutions. The variable transverse grids based on a moving mesh guideline [2,15] are more preferably for more reliable numerical approximations.

Example 4.2. Consider the same Gaussian beam initial function for $\kappa = 10$. We recover real, imaginary parts and modules of the field function E^σ from ϕ^σ, ψ^σ . A fixed nonuniform transverse mesh for (2.10) is utilized. Since the numerical solution is symmetric with respect to x - and y - axes in transverse directions, to reduce the graphic memory, we plot two-dimensional x -projections of the numerical solutions in Fig. 4.4. Wave propagation levels at $\sigma = 900, 950, 975$ and 1000 near the focusing position [9,12] are selected. It is evidential that the visible instability disturbances again occur, though in the current case they appear much later as compared with the situation in Example 4.1. A localized showing domain is used in simulations for better visualizations of the disturbances.

To see more details how an instability destroys the correct physical pattern of the numerical solution, we again show 3-dimensional views of the modules of E^{950} and E^{970} in Fig. 4.5. We may recall that they are similar to ϕ^{950} and ϕ^{970} , solutions of the eikonal transformation based splitting method (2.8), (2.9) or (2.10), respectively. Nonphysical disturbances eventually occur after a long time of computations using our method proposed, though the wave number, $\kappa = 10$, involved in this experiment is relatively large.

Example 4.3. In this example, we show several effective strategies to use together with the Peaceman–Rachford splitting method (2.8) and (2.9), or (2.10), on arbitrary grids. To this end, in Fig. 4.6, we plot contour maps of the numerical solution ϕ^σ, ψ^σ of (2.8), (2.9) at the 100th z -level. Both functions are symmetric with respect to the x - and y -axes. Their function values change rapidly around the central transverse area similar to that shown in Figs. 4.1–4.3. The last picture in Fig. 4.6 shows a successful application of the exponentially evolving grids (EEG) [2] used in the computational circumstance.

The adaptation is fulfilled in the following way: we first determine a dominant wave pattern to follow. This can be identified as the curvature of $\phi^{100}(x, 0), -\ell \leq x \leq \ell$, due to the symmetry of the wave function. Then the arc length of the above function is evaluated and divided into n segments. Finally, projections of these segments into the x -coordinate become our computational grids to use. In Fig. 4.7, we show the dominant curvature function $\phi = \phi^{100}(x, 0), -1 \leq x \leq 1$, a distribution of its corresponding grid steps, and ratios $h_k/h_{k+1}, k = 1, 2, \dots, n - 1$, acquired. Detailed information about the nonuniform grid step sizes and adaptive ratios are also given in Table 4.1.

Of course a wave pattern may not always be symmetric. As an illustration, in Fig. 4.8, we show nonuniform adaptive grids under another EEG strategy for a shifted optical wave pattern of the solutions ϕ^σ, ψ^σ of (2.8), (2.9). This slight shift is due to a degeneracy introduced to the Helmholtz equation problem [2]. Although adaptations demonstrated in Figs. 4.6–4.8 are primarily based on profiles of ϕ^σ rather than ψ^σ , the monitoring procedure can be conveniently allocated to any part of a targeted numerical solution, even its derivatives [2,10,15]. The sole reason of current mesh orientations is that the curvature structure of ϕ is much richer than that of ψ .

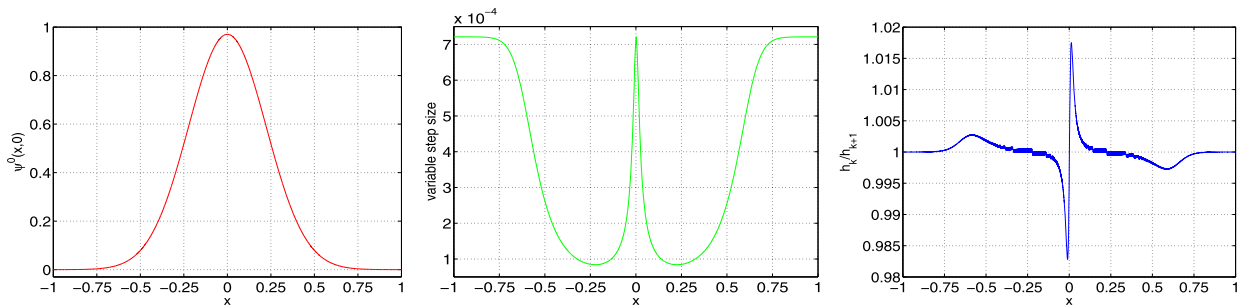


Fig. 4.7. An illustration of the variable grids corresponding to the circumstances. While the dominant nonlinear curvature function ϕ is shown on the left, the corresponding arc length based variable grid size distribution is in the middle. In addition, the adaptive grid step ratio distribution, which follows very well the smoothness constraint, is on the right.

Table 4.1
Adaptive step size and ratio ranges

$\min_{1 \leq k \leq n} h_k$	8.399606400996684e-05
$\max_{1 \leq k \leq n} h_k$	7.212705496510985e-04
$\min_{1 \leq k \leq n-1} h_k/h_{k+1}$	0.982810848890452
$\min_{1 \leq k \leq n-1} h_k/h_{k+1}$	1.017503421450693

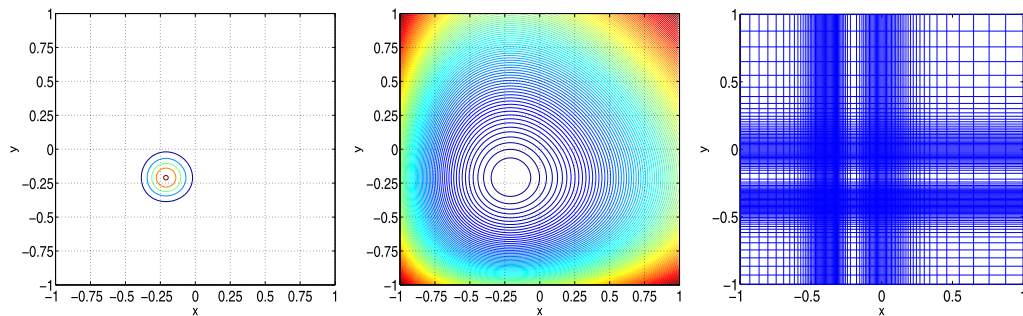


Fig. 4.8. Contour maps of a non-symmetric pair of ϕ^{100} (left) and ψ^{100} (center). The corresponding symmetric nonuniform grids (right) are also generated by an arc length adaptive formula via monitoring function [2]. The mesh follows nicely the shift and movement of wave solutions. The easy-to-compute variable transverse grids are more preferably for better numerical approximations.

5. Concluding remarks

Through a rigorous matrix spectrum analysis, this paper proves that the eikonal transformation based modified Peaceman–Rachford splitting method (2.8), (2.9), or (2.10), is asymptotically stable on arbitrary adaptive grids. The nonuniform finite difference method successfully removes high oscillations from the original paraxial wave equation (1.3), and provides a highly effective, efficient and reliable way for solving the underlying paraxial partial differential equation problem.

The analysis conducted in this paper can be further extended for examining similar oscillation-free algorithms, in particular those utilizing an eikonal, or ray, transformation. Other oscillatory optical beam or self-focusing wave problems, such as Kukhtarev systems for photorefractive waves, wave-material interaction models [1,3,8,9,12] and Maxwell's equations in large electromagnetic fields [4,12,17,22,28], may be considered.

Acknowledgements

The authors would like to thank the anonymous referees for their time, thorough comments and encouragements. Integrating their suggestions has undoubtedly elevated the quality and presentation of this paper.

The authors would also appreciate for the partial support through a Research Leave Award from Baylor University, and research grants # MYRG102 (Y1-L3)-FST13-SHW from University of Macau and # 105/2012/A3 from the FDCT of Macao.

References

- [1] Y.B. Band, *Light and Matter: Electromagnetism, Optics, Spectroscopy and Lasers*, John Wiley & Sons, West Sussex, 2006.

- [2] M.A. Beauregard, Q. Sheng, Solving degenerate quenching-combustion equations by an adaptive splitting method on evolving grids, *Comput. Struct.* 122 (2013) 33–43.
- [3] M.O. Bristeau, J. Erhel, P. Féat, R. Glowinski, J. Periaux, Solving the Helmholtz equation at high-wave numbers on a parallel computer with a shared virtual memory, *Int. J. High Perform. Comput. Appl.* 9 (1995) 18–28.
- [4] V.R. Chinni, C.R. Menyuk, P.K. Wai, Accurate solution of the paraxial wave equation using Richardson extrapolation, *IEEE Photonics Technol. Lett.* 6 (1994) 409–411.
- [5] M. Condon, A. Deaño, A. Iserles, On highly oscillatory problems arising in electronic engineering, *Modél. Math. Anal. Numér.* 43 (2009) 785–804.
- [6] B. Enquist, A. Fokas, E. Hairer, A. Iserles, *Highly Oscillatory Problems*, London Math. Soc., London, 2009.
- [7] V. Fedorchuk, V. Fedorchuk, On classification of symmetry reductions for the eikonal equation, *Symmetry* 8 (2016), <http://dx.doi.org/10.3390/sym8060051>.
- [8] G.D. Gillen, S. Guha, Modeling and propagation of near-field diffraction patterns: a more complete approach, *Am. J. Phys.* 72 (2004) 1195–1201.
- [9] G.D. Gillen, C.M. Seck, S. Guha, Analytical beam propagation model for clipped focused-Gaussian beams using vector diffraction theory, *Opt. Express* 18 (2010) 4023–4040.
- [10] L.P. Gonzalez, S. Guha, J.W. Rogers, Q. Sheng, An effective z -stretching method for paraxial light beam propagation simulations, *J. Comput. Phys.* 227 (2008) 7264–7278.
- [11] J.W. Goodman, *Introduction to Fourier Optics*, third edition, Roberts & Company Publishers, Denver, 2004.
- [12] S. Guha, Validity of the paraxial approximation in the focal region of a small- f -number lens, *Opt. Lett.* 26 (2001) 1598–1600.
- [13] S. Guha, A steepest descent approach for the eikonal equation in geometrical optics, Tech Report, AFRL/RXPJ 09-02-09, 2009.
- [14] S. Guha, L.P. Gonzalez, Q. Sheng, Description of light focusing by a spherical lens using diffraction integral method, *Proc. Appl. Math. Mech.* 7 (2008) 1023301–1023302.
- [15] W. Huang, R.D. Russell, *Adaptive Moving Mesh Methods*, Springer, Heidelberg and New York, 2012.
- [16] T. Jones, L.P. Gonzalez, S. Guha, Q. Sheng, A continuing exploration of decomposed compact methods for highly oscillatory wave problems, *J. Comput. Appl. Math.* 299 (2016) 207–220.
- [17] C. Pollock, M. Lipson, *Integrated Photonics*, Springer, Berlin and New York, 2003.
- [18] R.P. Ratowsky, J.A. Fleck, Accurate numerical solution of the Helmholtz equation by iterative Lanczos reduction, *Opt. Lett.* 16 (1991) 787–789.
- [19] Q. Sheng, ADI methods, in: *Encyclopedia of Applied and Computational Mathematics*, Springer Verlag GmbH, Heidelberg, 2015.
- [20] Q. Sheng, The legacy of ADI, LOD methods and an operator splitting for solving highly oscillatory wave problems, *Springer Proc. Math. Stat.* 171 (2016) 215–230.
- [21] Q. Sheng, S. Guha, L.P. Gonzalez, An exponential transformation based splitting method for fast computations of highly oscillatory solutions, *J. Comput. Appl. Math.* 235 (2011) 4452–4463.
- [22] Q. Sheng, H. Sun, On the stability of an oscillation-free ADI method for highly oscillatory wave equations, *Commun. Comput. Phys.* 12 (2012) 1275–1292.
- [23] Q. Sheng, H. Sun, Exponential splitting for n -dimensional paraxial Helmholtz equation with high wavenumbers, *Comput. Math. Appl.* 68 (2014) 1341–1354.
- [24] J. Trevelyan, M.E. Honnor, A numerical coordinate transformation for efficient evaluation of oscillatory integrals over wave boundary elements, *J. Integral Equ.* 21 (2009) 447–468.
- [25] J.A. Stratton, L.J. Chu, Diffraction theory of electromagnetic waves, *Phys. Rev.* 56 (1939) 99–107.
- [26] S.A. Üsküplü, M. Condon, A. Deaño, A. Iserles, Highly oscillatory diffusion-type equations, *J. Comput. Math.* 31 (2014) 549–572.
- [27] D. Xiu, J. Shen, An efficient spectral method for acoustic scattering from rough surfaces, *Commun. Comput. Phys.* 2 (2007) 54–72.
- [28] N.P. van der Aa, *The rigorous coupled-wave analysis*, Ph.D. dissertation, Faculteit Wiskunde & Informatica, Technische Universiteit Eindhoven, The Netherlands, 2007.
- [29] W.P. Zang, J.G. Tian, Z.B. Liu, W.Y. Zhou, F. Song, C.P. Zhang, Local one-dimensional approximation for fast simulation of Z -scan measurements with an arbitrary beam, *Appl. Opt.* 43 (2004) 4408–4414.